In this study, we first verified whether the different intratumoral accumulation pattern of [^{64}Cu]Cu-ATSM and [^{18}F]FDG is a common phenomenon shared by different types of tumors. We selected four mouse tumor cell lines of quite different origin to make tumor masses and studied the intratumoral distribution of [^{64}Cu]Cu-ATSM and [^{18}F]FDG using similar methods to the previous study [9]. Second, we examined the tumors immunohistologically, focusing on microblood vessels and proliferating cells that represent the source of the supply and consumption of oxygen, respectively. The abundance of apoptotic cells, which has been reported to increase under hypoxia [10–12], was also examined. We compared regions with high [^{64}Cu]Cu-ATSM and [^{18}F]FDG uptake and revealed the relationship between the regional characteristics and accumulation of the two tracers.

2. Materials and methods

2.1. Tracers

^{64}Cu was produced on a small biomedical cyclotron at the Biomedical Imaging Research Center in the University of Fukui, Japan, according to a published method [13]. [^{64}Cu]Cu-ATSM was synthesized by mixing 200-mM glycine buffer containing ^{64}Cu and H_2 ATSM in dimethly sulfoxide (1:100 by molar ration), as described previously [3]. The radiochemical purity of synthesized [^{64}Cu]Cu-ATSM was >99%, evaluated by HPLC (LC-10ADVP; Shimadzu, Kyoto, Japan) using a reversed phase column (Cosmosil 5C18-AR, 4.6×50 mm+4.6×150 mm; Nacalai Tesque, Kyoto, Japan) [14]. [^{18}F]FDG was synthesized by the method of Hamacher et al. [15] with an automated [^{18}F] FDG synthesizing system (JFE, Tokyo, Japan). The specific activity of [^{64}Cu]Cu-ATSM was 56 GBq/μmol, and that of [^{18}F]FDG was 20 to 50 GBq/μmol.

2.2. Animal models

Mice were treated in accordance with the animal treatment regulations of the University of Fukui throughout the experiments. The four mouse tumor cell lines used were B16 (melanoma), Meth-A (sarcoma), colon26 (adenocarcinoma) and LLC1 (Lewis lung carcinoma). Male mice, C57BL/6 and BALB/C, were obtained from Japan SLC (Shizuoka, Japan) at 6 weeks old and 20 to 25 g of body weight. The tumor cells, approximately 1×10^7 cells suspended in PBS, were injected into the hypodermis. B16 and LLC1 were implanted into C57BL/6, and Meth-A and colon26 into BALB/C mice. Three mice per cell line were prepared.

2.3. Autoradiography

At 4 weeks after the implantation of tumor cells, each mouse was injected intravenously with 74 MBq (2 mCi) [^{18}F]FDG and 0.37 MBq (10 μCi) [^{64}Cu]Cu-ATSM. Sixty minutes after the injection, the mice were sacrificed and the tumors were removed. The removed tumors were immediately covered with optimal cutting temperature (OCT) compound and frozen in methanol cooled with dry ice. They were divided into sections, and the cutting surfaces were flattened using a cryostat (Cryocut 1800, Leica, Wetzlar, Germany), then subjected to dual-tracer autoradiography [4]. [^{18}F]FDG images were acquired over 3 min, exposing the frozen sections to an imaging plate (BAS-MP 2040S; Fuji Photo Films, Japan) in a freezer. The imaging plate was scanned with a bioimaging analyzer (BAS-1500; Fuji Photo Films). After waiting 40 h for ^{18}F decay, [^{64}Cu]Cu-ATSM images were acquired over 45 h and the imaging plate was scanned. The distributions of [^{18}F]FDG and [^{64}Cu]Cu-ATSM were visualized by Mac-BAS v2.52 software (Fuji Photo Film). The contribution of ^{64}Cu radioactivity to the FDG image (the first autoradiography) was estimated to be around 1%, and the contribution of ^{18}F radioactivity to the Cu-ATSM image (the second exposure) was less than 0.1%. In each tumor section, the highest photostimulated luminescence region was classified as 100%, and the background was 0%. The 0% to 100% range was divided into four parts and colored red (75–100%), orange (50–75%), green (25–50%) and blue (0–25%), and the background was black. The colored image was saved in true color TIFF format.

2.4. Immunohistochemical staining

The frozen blocks used for the double tracer autoradiography were thawed, fixed in 10% neutral-buffered formalin and embedded in paraffin. The sections used for the immunohistochemical staining were made from the region within 50 μm from the surface exposed for autoradiography. After ^{64}Cu decay, immunohistochemical staining was carried out to detect proliferating cells, blood vessels and apoptotic cells using 2-μm-thick serial paraffin sections.

2.4.1. Proliferating cells

Ki67 is a nuclear protein expressed at all active phases of the cell cycle (G_1, S, G_2 and mitosis) with the highest expression in the G_2/M phase, but it is absent from the resting cells (G_0). The proliferating cell fraction can be determined immunohistochemically by using antibodies against Ki67 [16]. The sections were deparaffinized and rehydrated to detect proliferating cells, then endogenous peroxidase was blocked by 3% hydrogen peroxide. Antigen retrieval was carried out by microwaving for 25 min in 10-mM citrate buffer at pH 6. Nonspecific stain-blocking reagent (X0909, Dako Cytomation, Glostrup, Denmark) was applied for 20 min at room temperature (RT). The sections were then incubated overnight at 4°C with rat monoclonal antimouse Ki67 antigen antibody (M7249, Dako Cytomation) in 1:50 dilution with PBS. After washing with PBS, the sections were incubated with rabbit antirat biotinylated secondary antibody (E0468, Dako Cytomation) in 1:200 dilution with PBS for 30 min at RT, then incubated with streptavidin conjugated to horseradish peroxidase (streptavidin-HRP, K0673, Dako Cytomation) for 30 min at RT. Finally, the sections were incubated with 3,3′ -diaminobenzine tetrahydrochloride

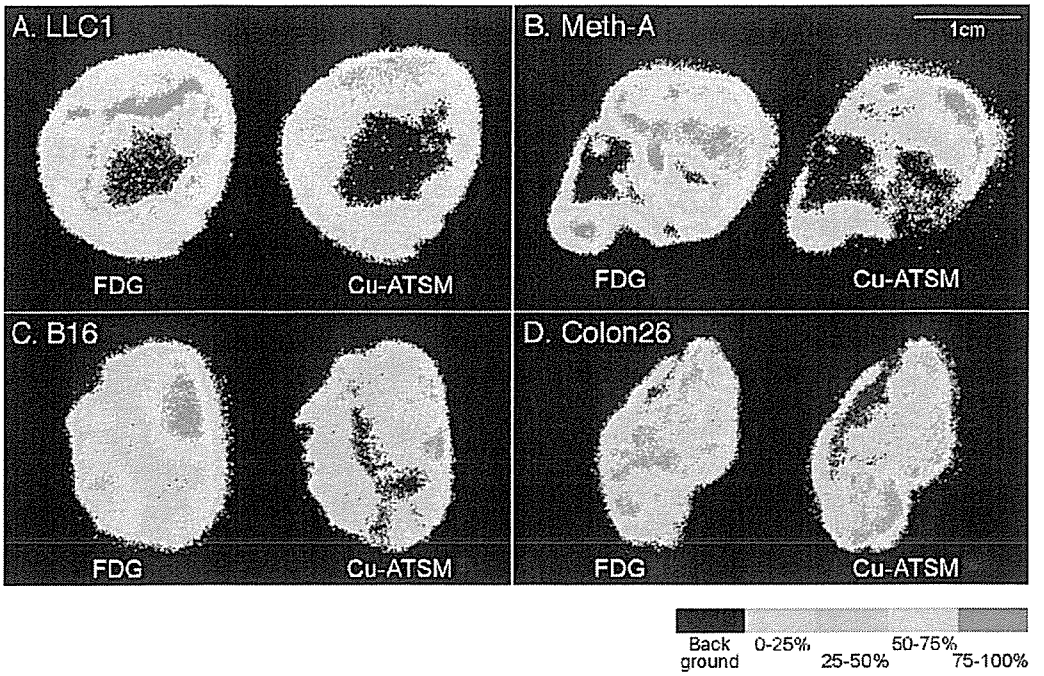

Fig. 1. Representative intratumoral distributions of ^{18}FDG and ^{64}Cu-ATSM in the tumor mass of LLC1(A), Meth-A(B), B16(C) and colon26(D) are shown. Autoradiographic images of ^{18}FDG and ^{64}Cu-ATSM were made from the same section.

solution (DAB Liquid System, Dako Cytomation) until suitable staining developed, then the nuclei were slightly counterstained with hematoxylin.

2.4.2. Blood vessels

CD34 is a cell glycoprotein expressed in the endothelial cells of small blood vessels [17]. To detect blood vessels in the sections, we used anti-CD34 antibody for B16 and colon26 tumors. The sections were deparaffinized and rehydrated, and endogenous peroxidase was blocked as described above. Antigen retrieval was performed for 15 min, and nonspecific staining was blocked as above. The sections were then incubated overnight at 4°C with rat antimouse CD34 antibody (HM1015; Hycult Biotechnology, Netherlands) in 1:20 dilution with PBS. After washing with PBS, the sections were incubated with rabbit antirat biotinylated secondary antibody (Dako Cytomation) in 1:100 dilution with PBS for 30 min at RT, and then incubated with streptavidin-HRP for 30 min at RT. The detection of peroxidase activity and the counterstaining were performed as described above.

von Willebrand factor (vWF) is synthesized by endothelial cells [18] and used for blood vessel staining. Because the anti-CD34 antibody did not work with Meth-A and LLC1 tumor sections because of high background staining, we used anti-vWF antibody for microvessel staining with Meth-A and LLC1 tumors. The sections were treated as described for CD34 staining, then incubated overnight at 4°C with polyclonal rabbit antimouse vWF antibody (A0082, Dako Cytomation) in 1:500 dilution with PBS. After washing with PBS, the sections were incubated with goat antirabbit immunoglobulin conjugated to peroxidase-labeled dextran polymer (Dako EnVision+, K4002, Dako Cytomation) for 30 min at RT. The peroxidase activity and the counterstaining were detected as described above.

2.4.3. Apoptotic cells

To evaluate apoptosis, we used a commercially available kit (ApopTag Peroxidase Kit, S7100; Chemicon, Temecula, CA), which uses the terminal deoxynucleotidyltransferase (TdT)-mediated dUTP nick end labeling method [19]. Briefly, after sections were deparaffinized and rehydrated, and endogenous peroxidase was blocked by 3% hydrogen peroxide, the sections were incubated with proteinase K (Wako, Japan) in 1:50 000 dilution with PBS for 30 min at 30°C. After rinsing with PBS, the sections were incubated with equilibration buffer at RT for 13 min, then with TdT enzyme and reaction buffer, and mixed at a 3:7 ratio, at 37°C for 60 min. The sections were then steeped in stop–wash buffer, prepared at 1:35 dilution with PBS, at 37°C for 30 min. After washing with PBS, the sections were incubated with anti-digoxigenin-peroxidase at RT for 30 min. Peroxidase activity and counterstaining were detected as described above.

2.5. Image analysis

Whole images of the serial sections stained for Ki67, CD34, vWF and apoptosis were captured by a scanner (Epson GT-8500) and saved in JPEG format. Composite images were made using Adobe Photoshop to compare the autoradiographic images with those of the stained sections. [^{64}Cu]Cu-ATSM and [^{18}F]FDG images were stacked in layers above the images of stained sections and made translucent. A composite image was made for each tumor

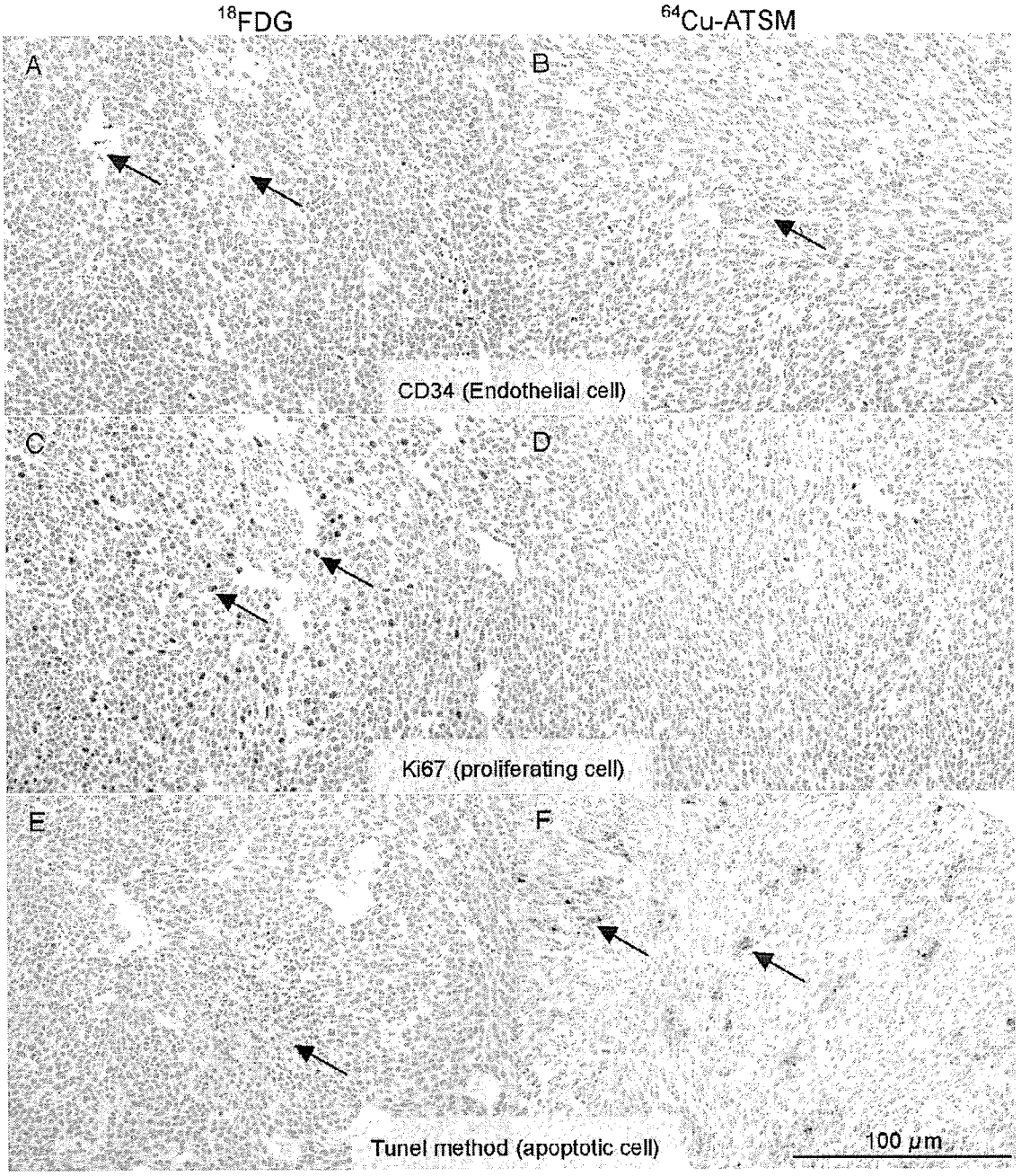

Fig. 2. Examples of immunohistochemical staining for CD34 (A, B), Ki67 (C, D) and Tunel (E, F) in colon26 sections at ×200. Panels A, C and E show regions with the highest ^{18}FDG accumulation. Panels B, D and F show regions with the highest ^{64}Cu-ATSM accumulation. Arrows indicate blood vessels (13 vessels) in panel A; single endothelial cells, which do not constitute the vessel, in panel B; and proliferating cells (198 cells) in panel C. Few proliferating cells (0 cells) are seen in D. In E, the arrow indicates necrosis. Few apoptotic cells are seen in E. In F, arrows indicate apoptotic cells (50 cells).

mass, and three composite images were quantified for each cell line. In each composite image, three areas from the region of each color for [^{64}Cu]Cu-ATSM and [^{18}F]FDG were analyzed. Digital images of the area (0.31 mm^2) were obtained at ×200 magnification using a microscope (Olympus BX50) mounted with a CCD camera and connected to a Windows computer. Proliferating cells, microblood vessels and apoptotic cells were counted manually on the computer monitor. The numbers of positively stained cells or microvessels in the nine areas (three areas from one section, one section from one mouse and three mice for one tumor cell line) were averaged for each different color indication level of [^{64}Cu]Cu-ATSM and [^{18}F]FDG accumulation.

2.6. Statistical analysis

Statistical analyses were performed with StatView software, Version 5.0. For comparison, the determination of correlation coefficients and the Mann–Whitney U test were applied. $P < .05$ was considered as statistically significant.

3. Results

3.1. Intratumoral distribution of [^{18}F]FDG and [^{64}Cu]Cu-ATSM

To analyze the intratumoral distribution of [^{18}F]FDG and [^{64}Cu]Cu-ATSM, we performed dual autoradiography with implanted mouse tumors of different origins. The representative images are shown in Fig. 1. [^{64}Cu]Cu-ATSM mainly accumulated at the edge of the tumors, and no accumulation was seen in the center where the cells were necrotic. On the other hand, the highest uptake region of [^{18}F]FDG was seen inner adjacent to that of [^{64}Cu]Cu-ATSM. The highest regions of [^{18}F]FDG and [^{64}Cu]Cu-ATSM, colored red, were distributed differently in all sections studied.

3.2. Microvessel density

To assess microvessel density (MVD), we counted the number of blood vessels per view in each region differentially colored according to the tracer accumulation. In the highest [^{18}F]FDG regions, abundant vessels were spreading into the tumor tissue and seemed to be functioning as blood vessels (Fig. 2A). Tumor cells near the vessels contained large and round nuclei, but small necrotic regions were frequently observed some distance from the blood vessels.

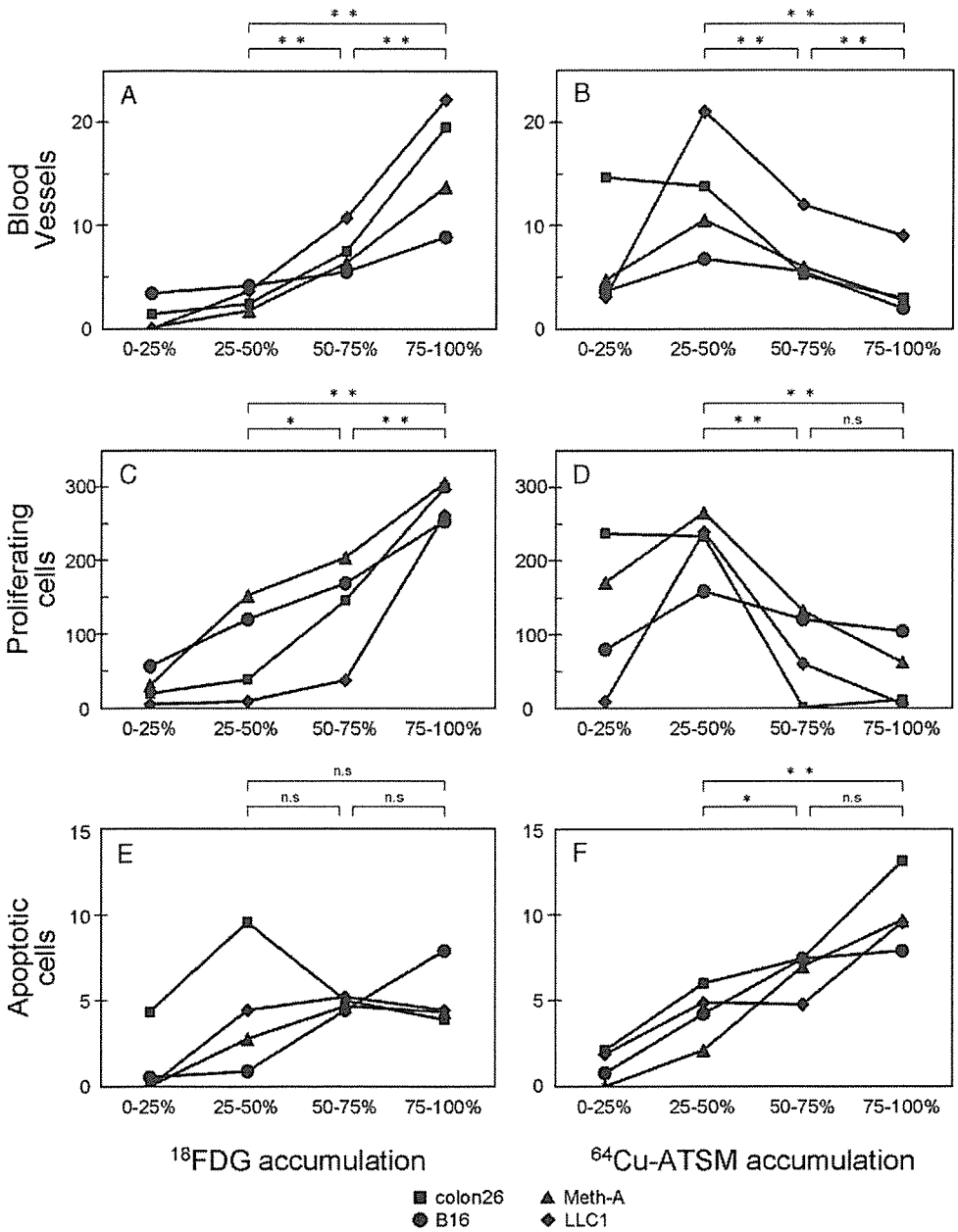

Fig. 3. These graphs show the number of blood vessels, proliferating cells and apoptotic cells compared with the intratumoral distribution of ^{18}FDG/^{64}Cu-ATSM. Three tumor sections were quantified for each cell line. Each point represents the average of positively stained cells in nine views from each region classified by the degree of ^{18}FDG or ^{64}Cu-ATSM accumulation. There were approximately 2000 tumor cells in the microscope view. Statistical analyses were performed by summarizing four cell lines (**$P < .01$, *$P < .05$, ns indicates not significant).

The vessel count in the highest uptake region of [^{64}Cu]Cu-ATSM was remarkably less than that of [^{18}F]FDG, but there was no necrosis, and abundant viable tumor cells were seen (Fig. 2B). The tumor cells in the highest [^{64}Cu]Cu-ATSM region had smaller nuclei and lower chromatin concentration compared with the highest [^{18}F]FDG region.

The relationship between MVD and the accumulation of two tracers in each tumor mass are shown in Fig. 3A and B, in which each point represents the mean of nine blood vessel counts from each region. Each graph summarizes the data of 144 views in 48 regions from 12 tumor sections. Positive correlation was found between [^{18}F]FDG and MVD in all four tumor cell lines (Fig. 3A). On the other hand, the number of vessels decreased with the increase in [^{64}Cu]Cu-ATSM uptake, excluding the lowest [^{64}Cu]Cu-ATSM uptake region (Fig. 3B). In all cell lines except colon26, the MVD was very low in the lowest [^{64}Cu]Cu-ATSM region, where most tumor cells were necrotic with a shrunken nucleus. For colon26, MVD was relatively high compared with the other tumors in the lowest [^{64}Cu]Cu-ATSM region, which contained abundant blood vessels and viable tumor cells.

3.3. Cell proliferation

To evaluate cell proliferation in each section, we performed Ki67 immunohistochemistry. Positive nuclear staining of Ki67 in tumor cells was abundantly observed in the highest [^{18}F]FDG region, but it was hardly observed in that of [^{64}Cu]Cu-ATSM (Fig. 2C and D). Similar to MVD, the number of Ki67 positive cells increased with [^{18}F]FDG uptake (Fig. 3C) and decreased with [^{64}Cu]Cu-ATSM uptake (Fig. 3D). Cell proliferation was active in the lowest [^{64}Cu]Cu-ATSM region only in the colon26 sections.

3.4. Apoptosis

To assess apoptosis, we used an ApopTag Peroxidase Kit to stain the sections, and the number of apoptotic cells was counted. In the highest [^{18}F]FDG region, few apoptotic cells were observed (Fig. 2E). The regions in which tumor cells with shrunken nuclei gathered were not stained, indicating that the regions were necrotic, not apoptotic. In the highest uptake region of [^{64}Cu]Cu-ATSM, more apoptotic cells were seen compared with the [^{18}F]FDG region (Fig. 2F), although the number of apoptotic cells was less than 1% of all tumor cells. A positive correlation was found between the apoptotic cell number and [^{64}Cu]Cu-ATSM accumulation (Fig. 3F), but no correlation was found between the apoptotic cell number and [^{18}F]FDG accumulation (Fig. 3E).

4. Discussion

In this study, we demonstrated that [^{64}Cu]Cu-ATSM and [^{18}F]FDG were distributed with different gradation of the tumor mass from all four mouse tumor cell lines (Fig. 1). At the macroscopic level, the tumor cells of LLC1 and colon26 formed a concentric circular shape around the necrosis, with the highest [^{64}Cu]Cu-ATSM uptake seen in the outer region and the highest [^{18}F]FDG uptake in the inner region of the sections (Fig. 1A and D). On the other hand, with Meth-A and B16, the tumor cells tended to form multiple tubercular shapes when the tumor size increased and the section diameter exceeded 2 cm. In these sections, [^{64}Cu]Cu-ATSM was found at highest in the outer region of the tubercles, and [^{18}F]FDG was found at highest in the inner region of the tubercles bordering the region accumulating [^{64}Cu]Cu-ATSM (Fig. 1B and C). Thus, it seemed to be a phenomenon shared by various tumors that [^{18}F]FDG and [^{64}Cu]Cu-ATSM were accumulated with different gradation, forming a unique pattern of a high [^{64}Cu]Cu-ATSM region surrounding a high [^{18}F]FDG region within a tumor mass.

In the high [^{18}F]FDG region, MVD was high and abundant proliferating cells were observed (Fig. 2A and C). A positive correlation was found between [^{18}F]FDG accumulation and the number of proliferating cells (Fig. 3A). The high [^{18}F]FDG regions seemed to be under normal oxygen tension, because MVD was quite high and [^{64}Cu]Cu-ATSM, a hypoxic marker, did not accumulate in these regions. These findings indicate that [^{18}F]FDG was mainly taken up by proliferating tumor cells, which are not so hypoxic that [^{64}Cu]Cu-ATSM will accumulate. In these regions, cell death was mainly from necrosis, which could be caused by environmental aggravation. Because of the abnormality of tumor vasculature and very active cell proliferation, severe disturbance to the microcirculation and oxygen supply would occur, leading to tumor cell death at some distance from the vessels. Tumor cells in the high [^{18}F]FDG region seemed to have characteristics specific to malignant tumors, in which tumor cells proliferate without limit until they die. However, there are data by Pugachev et al. [20] that suggest that the higher FDG uptake was indicative of tumor hypoxia, but neither blood flow nor cellular proliferation, with the nude mice bearing Dunning prostate tumor. There are also several articles supporting the positive correlation between FDG uptake and blood flow in experimental and clinical settings [21–23]. The discrepancy can be resulted from the difference in the tumor types, difference in the techniques to evaluate the vascularity or blood flow (perfusion by Hoechst, microvessel density and O-15 H_2O, etc.), difference in the resolution of the images or difference in some other conditions.

In the highest [^{64}Cu]Cu-ATSM regions, MVD was very low and few proliferating cells were observed (Fig. 2B and D). A negative correlation was found between MVD and [^{64}Cu]Cu-ATSM accumulation (Fig. 3B), in agreement with the hypothesis that [^{64}Cu]Cu-ATSM accumulates in hypoxic regions. These regions had few necrotic cells and mostly consisted of viable tumor cells whose nuclei were uniform but smaller than those found in the highest [^{18}F]FDG regions. It has been reported that some tumor cells survive hypoxia in environmental aggravation but are arrested in the G_0 or G_1 phase [24,25]. There seem to be similarities between surviving tumor cells and cells in the

highest [^{64}Cu]Cu-ATSM region. The high [^{64}Cu]Cu-ATSM region can be described as hypovascular, and the cell cycle-arrested region is where oxygen consumption and glucose metabolism are reduced and tumor cells quietly wait for the environment to improve. In addition, a positive correlation was found between [^{64}Cu]Cu-ATSM accumulation and the number of apoptotic cells (Fig. 3F). It should be noted that the number of apoptotic cells in the highest [^{64}Cu]Cu-ATSM region, even where apoptotic cells were most frequently observed, was less than 1% of all tumor cells, although it was reported that hypoxia can induce apoptotic cell death in tumor cells [10–12]. Tumor cells in the high [^{64}Cu]Cu-ATSM region seem to have atypical characteristics similar to malignant tumors: they can maintain self-control. They respond to environmental changes and stop cell proliferation, and when they die, they die of apoptosis, a programmed cell death.

In our study, it was revealed that there are regions containing cells of different phenotypes in the same tumor mass, which can be distinguished using PET tracers [^{18}F]FDG and [^{64}Cu]Cu-ATSM. As the tumor mass is formed by cells from a single cell line, different phenotypes should have resulted from adaptation to the intratumoral microenvironment, such as hypoxia and malnutrition. Radiotherapy and some chemotherapy are effective in malignant tumors against normoxic and actively dividing cells, but are less effective against cells with low oxygen tension and arrested cell cycle [26,27]. Our study implies that tumor cells in the high [^{18}F]FDG region are sensitive to therapy, but those in the high [^{64}Cu]Cu-ATSM region are resistant.

It was also interesting that lone endothelial cells were often detected in the highest [^{64}Cu]Cu-ATSM regions (Fig. 2B). Hypoxia induces angiogenic factors such as vascular endothelial growth factor and platelet-derived endothelial cell growth factor [28,29]. If endothelial cells grow and form functional blood vessels, the environment in this region will be improved and tumor cells may start to proliferate. It has been reported that, after reoxygenation, tumor cells adapting to chronic hypoxia resume cell cycle progression with acquired resistance against radiation and anticancer drugs [30–32]. Tumor cells in the high [^{64}Cu]Cu-ATSM region are highly likely to turn into such death-resistant cells.

Our study indicated that the high [^{18}F]FDG region is where tumor cells actively proliferate and should receive immediate anticancer treatment, whereas the high [^{64}Cu]Cu-ATSM region is likely to be less sensitive to conventional antitumor treatment and needs more intensive and aggressive therapy. In a clinical PET study with [^{60}Cu]Cu-ATSM, tumors with high [^{60}Cu]Cu-ATSM accumulation responded poorly to therapy, and such tumors tended to develop local recurrence and lymph node metastasis [33,34]. Those reports confirm the ability of [^{60}Cu]Cu-ATSM PET to predict the tumor response to therapy and the prognosis, and support our view that the high Cu-ATSM region responds poorly to conventional therapy and needs aggressive treatment. As an intensive radiotherapy to the hypoxic region, hypoxia imaging (Cu-ATSM)-guided intensity-modulated radiation therapy has been performed for head-and-neck cancer patients [35]. Higher doses of radiation to the hypoxic region can overcome hypoxic resistance and increase the anticancer effect with minimal normal tissue complications.

Cu-ATSM itself has potential as an internal radiotherapy agent directly targeting such hypoxic and cell cycle-arrested regions when labeled with β^--emitting radioisotopes such as ^{64}Cu or ^{67}Cu. In animal models with a tumor, [^{64}Cu]Cu-ATSM could improve the survival time without acute toxicity [36,37]. When a sufficient radiation dose of [^{64}Cu]Cu-ATSM was taken up into the tumor cells, apoptotic cell death was induced because of DNA damage by radiation from ^{64}Cu inside the cells [38]. Because the β^- particle, the main cytotoxic agent of ^{64}Cu, penetrates tissue to several hundred micrometers, the cytotoxic effect of ^{64}Cu expands to neighboring cells, which will increase the anticancer effect.

5. Conclusion

Both [^{18}F]FDG and [^{64}Cu]Cu-ATSM provide important information about tumors, although the accumulation of each tracer indicates different characteristics of the tumor tissue. Information on the regional characteristics of tumors by [^{64}Cu]Cu-ATSM and [^{18}F]FDG PET will enable us to make finely tuned and effective treatment plans for tumors, especially when they are hypoxic and resistant to conventional therapy.

Acknowledgments

This study was partly supported by KAKENHI, a grant-in-aid for Scientific Research from the Ministry of Education, Culture, Sports, Science and Technology (MEXT) Japan, a 21st Century COE program "Biomedical Imaging Technology Integration Program" from Japan Society of the Promotion of Science (JSPS) and the Research and Development Project Aimed at Economic Revitalization (Leading Project) "Research and Development of Technology for Measuring Vital Functions Merged with Optical Technology" from MEXT Japan.

References

[1] Pitson G, Fyles A, Milosevic M, Wylie J, Pintilie M, Hill R. Tumor size and oxygenation are independent predictors of nodal diseases in patients with cervix cancer. Int J Radiat Oncol Biol Phys 2001;51: 699–703.
[2] Brown JM. The hypoxic cell: a target for selective cancer therapy — eighteenth Bruce F. Cain Memorial Award lecture. Cancer Res 1999;59:5863–70.
[3] Fujibayashi Y, Taniuchi H, Yonekura Y, Ohtani H, Konishi J, Yokoyama A. Copper-62-ATSM: a new hypoxia imaging agent with high membrane permeability and low redox potential. J Nucl Med 1997;38:1155–60.

[4] Fujibayashi Y, Cutler CS, Anderson CJ, et al. Comparative studies of Cu-64-ATSM and C-11-acetate in an acute myocardial infarction model: ex vivo imaging of hypoxia in rats. Nucl Med Biol 1999;26: 117–21.
[5] O'donoghue JA, Zanzonico P, Pugachev A, et al. Assessment of regional tumor hypoxia using (18)F-fluoromisonidazole and (64)Cu(II)-diacetyl-bis(N4-methylthiosemicarbazone) positron emission tomography: comparative study featuring microPET imaging, Po(2) probe measurement, autoradiography, and fluorescent microscopy in the R3327-AT and FaDu rat tumor models. Int J Radiat Oncol Biol Phys 2005;61:1493–502.
[6] Burgman P, Odonoghue JA, Humm JL, Ling CC. Hypoxia-Induced increase in FDG uptake in MCF7 cells. J Nucl Med 2001;42:170–5.
[7] Dearling JL, Flynn AA, Sutcliffe-Goulden J, et al. Analysis of the regional uptake of radiolabeled deoxyglucose analogs in human tumor xenografts. J Nucl Med 2004;45:101–7.
[8] Zhao S, Kuge Y, Mochizuki T, Takahashi T, et al. Biologic correlates of intratumoral heterogeneity in 18F-FDG distribution with regional expression of glucose transporters and hexokinase-II in experimental tumor. J Nucl Med 2005;46:675–82.
[9] Obata A, Yoshimoto M, Kasamatsu S, et al. Intra-tumoral distribution of (64)Cu-ATSM: a comparison study with FDG. Nucl Med Biol 2003;30:529–34.
[10] Graeber TG, Osmanian C, Jacks T, et al. Hypoxia-mediated selection of cells with diminished apoptotic potential in solid tumours. Nature 1996;379:88–91.
[11] Nagarajah NS, Vigneswaran N, Zacharias W. Hypoxia-mediated apoptosis in oral carcinoma cells occurs via two independent pathways. Mol Cancer 2004;3:38.
[12] Pan Y, Oprysko PR, Asham AM, Koch CJ, Simon MC. p53 cannot be induced by hypoxia alone but responds to the hypoxic microenvironment. Oncogene 2004;23:4975–83.
[13] Obata A, Kasamatsu S, McCarthy DW, et al. Production of therapeutic quantities of (64)Cu using a 12 MeV cyclotron. Nucl Med Biol 2003; 30:535–9.
[14] Obata A, Yoshimi E, Waki A, et al. Retention mechanism of hypoxia selective nuclear imaging/radiotherapeutic agent Cu-diacetyl-bis(N4-methylthiosemicarbazone) (Cu-ATSM) in tumor cells. Ann Nucl Med 2001;15:499–504.
[15] Hamacher K, Coenen HH, Stocklin G. Efficient stereospecific synthesis of no-carrier-added 2-[18F]-fluoro-2-deoxy-D-glucose using aminopolyether supported nucleophilic substitution. J Nucl Med 1986;27:235–8.
[16] Scholzen T, Gerdes J. The Ki-67 protein: from the known and the unknown. J Cell Physiol 2000;182:311–22.
[17] Fujieda S, Sunaga H, Tsuzuki H, Tanaka N, Saito H. Expression of platelet-derived endothelial cell growth factor in oral and oropharyngeal carcinoma. Clin Cancer Res 1998;4:1583–90.
[18] Sporn LA, Chavin SI, Marder VJ, Wagner DD. Biosynthesis of von Willebrand protein by human megakaryocytes. J Clin Invest 1985; 76:1102–6.
[19] Fujieda S, Inuzuka M, Tanaka N, et al. Expression of p27 is associated with Bax expression and spontaneous apoptosis in oral and oropharyngeal carcinoma. Int J Cancer 1999;84:315–20.
[20] Pugachev A, Ruan S, Carlin S, et al. Dependence of FDG uptake on tumor microenvironment. Int J Radiat Oncol Biol Phys 2005;62: 545–53.
[21] Bos R, van Der Hoeven JJ, van Der Wall E, et al. Biologic correlates of (18)fluorodeoxyglucose uptake in human breast cancer measured by positron emission tomography. J Clin Oncol 2002;20: 379–87.
[22] Zasadny KR, Tatsumi M, Wahl RL. FDG metabolism and uptake versus blood flow in women with untreated primary breast cancers. Eur J Nucl Med Mol Imaging 2003;30:274–80.
[23] Schroeder T, Yuan H, Viglianti BL, et al. Spatial heterogeneity and oxygen dependence of glucose consumption in R3230Ac and fibrosarcomas of the Fischer 344 rat. Cancer Res 2005;65: 5163–71.
[24] Amellem O, Sandvik JA, Stokke T, Pettersen EO. The retinoblastoma protein-associated cell cycle arrest in S-phase under moderate hypoxia is disrupted in cells expressing HPV18 E7 oncoprotein. Br J Cancer 1998;77:862–72.
[25] Webster L, Hodgkiss RJ, Wilson GD. Cell cycle distribution of hypoxia and progression of hypoxic tumour cells in vivo. Br J Cancer 1998;77:227–34.
[26] Cuisnier O, Serduc R, Lavieille JP, Longuet M, Reyt E, Riva C. Chronic hypoxia protects against gamma-irradiation-induced apoptosis by inducing bcl-2 up-regulation and inhibiting mitochondrial translocation and conformational change of bax protein. Int J Oncol 2003;23:1033–41.
[27] Yokoi K, Fidler IJ. Hypoxia increases resistance of human pancreatic cancer cells to apoptosis induced by gemcitabine. Clin Cancer Res 2004;10:2299–306.
[28] Koong AC, Denko NC, Hudson KM, et al. Candidate genes for the hypoxic tumor phenotype. Cancer Res 2000;60:883–7.
[29] Sipos B, Weber D, Ungefroren H, et al. Vascular endothelial growth factor mediated angiogenic potential of pancreatic ductal carcinomas enhanced by hypoxia: an in vitro and in vivo study. Int J Cancer 2002;102:592–600.
[30] Kinoshita M, Johnson DL, Shatney CH, Lee YL, Mochizuki H. Cancer cells surviving hypoxia obtain hypoxia resistance and maintain anti-apoptotic potential under reoxygenation. Int J Cancer 2001;91: 322–6.
[31] Koritzinsky M, Wouters BG, Amellem O, Pettersen EO. Cell cycle progression and radiation survival following prolonged hypoxia and re-oxygenation. Int J Radiat Biol 2001;77:319–28.
[32] Dong Z, Wang J. Hypoxia selection of death-resistant cells. A role for Bcl-X(L). J Biol Chem 2004;279:9215–21.
[33] Dehdashti F, Mintun MA, Lewis JS, et al. In vivo assessment of tumor hypoxia in lung cancer with 60Cu-ATSM. Eur J Nucl Med Mol Imaging 2003;30:844–50.
[34] Dehdashti F, Grigsby PW, Mintun MA, Lewis JS, Siegel BA, Welch MJ. Assessing tumor hypoxia in cervical cancer by positron emission tomography with 60Cu-ATSM: relationship to therapeutic response — a preliminary report. Int J Radiat Oncol Biol Phys 2003;55:1233–8.
[35] Chao KS, Bosch WR, Mutic S, et al. A novel approach to overcome hypoxic tumor resistance: Cu-ATSM-guided intensity-modulated radiation therapy. Int J Radiat Oncol Biol Phys 2001;49:1171–82.
[36] Lewis J, Laforest R, Buettner T, et al. Copper-64-diacetyl-bis(N4-methylthiosemicarbazone): an agent for radiotherapy. Proc Natl Acad Sci U S A 2001;98:1206–11.
[37] Aft RL, Lewis JS, Zhang F, Kim J, Welch MJ. Enhancing targeted radiotherapy by copper(II)diacetyl-bis(N4-methylthiosemicarbazone) using 2-deoxy-D-glucose. Cancer Res 2003;63:5496–504.
[38] Obata A, Kasamatsu S, Lewis JS, et al. Basic characterization of 64Cu-ATSM as a radiotherapy agent. Nucl Med Biol 2005; 32:21–8.

資料(5)

Available online at www.sciencedirect.com

SCIENCE DIRECT

Nuclear Medicine and Biology 33 (2006) 153–158

NUCLEAR MEDICINE — AND — BIOLOGY

www.elsevier.com/locate/nucmedbio

Technical note

New approach to fully automated synthesis of sodium [^{18}F]fluoroacetate — a simple and fast method using a commercial synthesizer

Li-Quan Sun[a], Tetsuya Mori[a], Carmen S. Dence[b], Datta E. Ponde[b], Michael J. Welch[b], Takako Furukawa[a], Yoshiharu Yonekura[a], Yasuhisa Fujibayashi[a,*]

[a]*Biomedical Imaging Research Center, University of Fukui, Yoshida, Fukui 910-1193, Japan*

[b]*Division of Radiological Sciences, Mallinckrodt Institute of Radiology, Washington University School of Medicine, St. Louis, MO 63110, USA*

Received 27 April 2005; received in revised form 6 July 2005; accepted 7 July 2005

Abstract

A simple, rapid and fully automated preparation of sodium [^{18}F]fluoroacetate has been developed by taking advantage of the similarities between the reaction pathways of [^{18}F]fluoroacetate and [^{18}F]-2-fluoro-deoxyglucose (FDG). The automated synthesis of sodium [^{18}F]fluoroacetate was achieved with a commercial [^{18}F]FDG synthesizer, the TRACERlab MX_{FDG}. The method produced the desired compound in a short synthesis time (32 min) and with a high and reproducible radiochemical yield (50.2±4.8%, decay corrected). The radiochemical purity of sodium [^{18}F]fluoroacetate was greater than 99%.

Keywords: Sodium [^{18}F]fluoroacetate; Ethyl [^{18}F]fluoroacetate; Automated synthesis; Commercial synthesizer; PET tracer

1. Introduction

Sodium fluoroacetate (sodium monofluoroacetate, Compound 1080) is well known as a salt with very high mammalian toxicity and is often used as a rodenticide or insecticide [1,2]. This salt is metabolized to fluorocitrate, which cannot be further metabolized to carbon dioxide and blocks the tricarboxylic acid cycle in the body [3,4]. Fluorine-18-labeled sodium fluoroacetate, like [^{11}C]acetate, has been used as a tracer for positron emission tomography (PET) to study myocardial metabolism and cerebral oxidative metabolism [5]. Sodium [^{18}F]fluoroacetate has a longer half-life than [^{11}C]acetate, so it should facilitate diagnostic studies by PET. Recent studies using sodium [^{18}F]fluoroacetate as a tumor imaging agent have been reported, and the results suggested that defluorination of sodium [^{18}F]fluoroacetate was species dependent and occurred in rodents but not in primates [6]. Sodium [^{18}F]fluoroacetate has also been reported to be a useful PET tracer for prostate cancer imaging [7]. It had a high sensitivity for detection of recurrent cancer in prostate [7] and provided higher tumor-to-background ratio than [^{11}C]acetate [6–8].

To realize sodium [^{18}F]fluoroacetate's potential in PET imaging, an automated synthesis carried out in a short period and with a high yield is necessary. In the last decade, several groups reported the preparation of sodium (or potassium) [^{18}F]fluoroacetate [9–12]. However, all of these needed a long synthesis time (>60 min) and provided a low radiochemical yield (<34%). As a result, these methods are unlikely to fulfill the high demand for the radiopharmaceutical if used routinely. We observed that the chemical steps to prepare sodium [^{18}F]fluoroacetate were similar to those used to prepare [^{18}F]-2-fluoro-deoxyglucose (FDG) [13]. Therefore, the instrumentation used in a [^{18}F]FDG synthesis should be able to produce sodium [^{18}F]fluoroacetate. Many automated [^{18}F]FDG synthesizers are commercially available today, each with individual characteristics and advantages. Among them, the TRACERlab MX_{FDG}, designed by GE Medical Systems (Liege, Belgium), was reported to provide a final injection solution of [^{18}F]FDG in a short time (25 min) from the end of bombardment (EOB) with a yield of more than 60% [14]. Therefore, we attempted to utilize

* Corresponding author. Tel.: +81 776 618430; fax: +81 776 61 8170.
E-mail address: yfuji@fmsrsa.fukui-med.ac.jp (Y. Fujibayashi).

0969-8051/$ – see front matter © 2006 Published by Elsevier Inc.
doi:10.1016/j.nucmedbio.2005.07.005

the TRACERlab MX_{FDG} for our fully automatic synthesis of sodium [^{18}F]fluoroacetate. Only minimal modifications were needed to synthesize sodium [^{18}F]fluoroacetate, and these modifications did not affect its intrinsic function as a [^{18}F]FDG synthesizer.

We have established a new automated method to prepare sodium [^{18}F]fluoroacetate using the TRACERlab MX_{FDG}, the complex of $K^{18}F$ and kryptofix 2.2.2 as nucleophile for the fluorination and ethyl *O*-mesyl-glycolate as the precursor.

2. Experiments

2.1. Materials and apparatuses

Ethyl glycolate and methanesulfonyl chloride were obtained from Tokyo Kasei Kogyo (TCI, Tokyo, Japan). Ethyl fluoroacetate and sodium fluoroacetate (as reference standards) were purchased from Wako Industries (Tokyo, Japan). Potassium carbonate, sodium hydroxide, anhydrous magnesium sulfate, hydrochloric acid, anhydrous acetonitrile and methylene chloride were purchased from Sigma-Aldrich Japan K.K. (Tokyo, Japan). Triethylamine and sodium bicarbonate were purchased from Kanto Kagaku (Osaka, Japan). Ethanol [99.5% for high-pressure liquid chromatography (HPLC)] was purchased from Nacalai Tesque (Kyoto, Japan). All reagents and solvents were of the highest purity available and used without further purification unless specifically stated. Sep-Pak QMA Light cartridges, C18 cartridges, Alumina-N cartridges and Oasis HLB Plus cartridges were purchased from Waters (Milford, MA, USA).

Analytical HPLC was performed on a Waters 600E system equipped with Waters 490E programmable multi-wavelength UV detector set at 210 nm and a Bioscan Flow counter (Washington, DC, USA). A reversed phase Hydrosphere C_{18} column (4.6×150 mm, YMC, Kyoto, Japan) was used with C_2H_5OH/H_2O (10/90) as the liquid phase at a flow rate of 1.0 ml/min.

Gas chromatography (GC) was performed using a Shimadzu 14A system equipped with a flame ionization detector. NMR spectra were obtained for solutions in acetonitrile-d_3, using a JEOL's JNM-400 NMR spectrometer (Tokyo, Japan). Radiometric thin-layer chromatography (TLC) was performed in a developing solvent of CH_3CN/H_2O (95/5) with 0.25 mm Silica Gel 60 Sheets F_{254} purchased from Nacalai Tesque. The TLC plates were analyzed using a Bioscan System AR-2000 imaging scanner (Washington, DC, USA).

Millex GS-vented 0.22-μm sterile filters were obtained from Millipore (Bedford, MA, USA). The LAL kits were purchased from Wako Industries. The pH of the solution was measured using a digital pH meter from Nidden (Tokyo, Japan). The disposable kits were purchased from GE Medical Systems. No-carrier-added [^{18}F]fluoride was produced via the ^{18}O (p, n) ^{18}F reaction in a CTI RDS-eclipse cyclotron (11.0 MeV protons) on an enriched ^{18}O water target. The enriched ^{18}O water (atom 97%+) was purchased from Rotem Ind. (Beer Sheva, Israel).

2.2. Modifications to the TRACERlab MX_{FDG}

As the TRACERlab MX_{FDG} was designed solely for the production of [^{18}F]FDG, some modifications were required

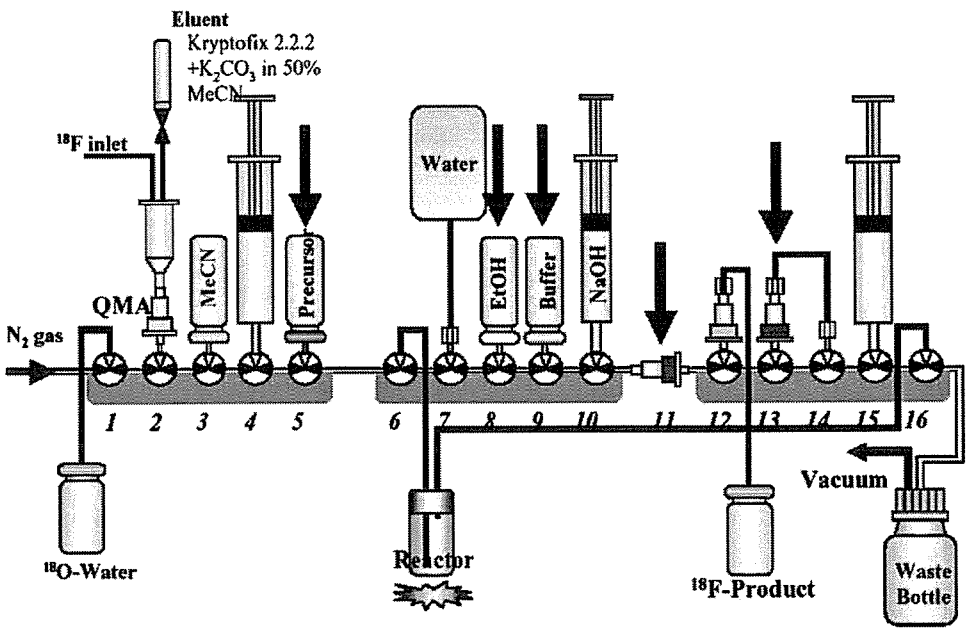

Fig. 1. Schematic diagram of TRACERlab MX_{FDG} for the preparation of [^{18}F]FDG. One Sep-Pak C-18 cartridge was placed at position 11 and another at position 13. The arrows indicate the parts to be replaced for the preparation of sodium [^{18}F]fluoroacetate.

for the preparation of sodium [^{18}F]fluoroacetate. The standard disposable kit and the arrangement of chemical reagents for the preparation of [^{18}F]FDG are shown schematically in Fig. 1. The disposable kit and the arrangement of chemical reagents after the necessary changes for the preparation of sodium [^{18}F]fluoroacetate are shown in Fig. 2. Other parts were not altered except for those documented in Table 1.

A new program file was written to control the automated synthesis of sodium [^{18}F]fluoroacetate. This program is similar to that used for [^{18}F]FDG synthesis, except for changes in the labeling reaction time (from 1 to 5 min), the reaction temperature (from 85°C to 105°C) and the hydrolysis reaction time for the intermediate (from 2 to 5.5 min).

2.3. Preparation of ethyl O-mesyl-glycolate (ethyl α-methanesulfonyl-glycolate)

The synthesis of ethyl *O*-mesyl-glycolate was accomplished following previous methods [9,15] with some modifications. Ethyl glycolate (5.0 g, 48.0 mmol) and methanesulfonyl chloride (6.5 g, 56.7 mmol) were dissolved in 50 ml of methylene chloride in a 200-ml round bottom flask. The solution was cooled to 0°C and triethylamine (5.0 ml, 35.8 mmol) was added dropwise with stirring. After stirring for 80 min at room temperature, the reaction mixture was extracted with ice-cold 1.0 M HCl (70 ml). The organic layer was washed twice with ice-cold water (70 ml) and dried over anhydrous magnesium sulfate. The solution was concentrated by a rotary evaporator and further distilled under reduced pressure. A colorless liquid (6.2 g) was collected at 149°C and 12.0 mm Hg. The liquid was identified as ethyl *O*-mesyl-glycolate with 70.1% yield. ^{1}H NMR (400 MHz, $CDCl_3$, TMS): δ 1.31 (t, 3H, J=7 Hz), 3.22 (s, 3H), 4.25 (q, 2H, J=7 Hz), 4.76 (s, 2H [16]).

Table 1
Content changes performed in the TRACERlab MX_{FDG} from [^{18}F]FDG to sodium [^{18}F]fluoroacetate syntheses

Position	[^{18}F]FDG	[^{18}F]fluoroacetate
3	CH_3CN (7 ml)	CH_3CN (3.5 ml)
5	Mannose triflate	Ethyl *O*-mesyl-glycolate
8	CH_3CH_2OH	$NaHCO_3$ (aq)
9	Buffer	1.0 M HCl (3.0 ml)
10	2.0 M NaOH (1.0 ml)	1.0 M NaOH (2.7 ml)
11	Sep-Pak C18 (X 1)	Oasis HLB Plus (X 1)
13	Sep-Pak C18 (X 1)	Oasis HLB Plus (X 3)

2.4. Preparation of sodium [^{18}F]fluoroacetate

Fluorine-18-labeled sodium fluoroacetate was synthesized by a nucleophilic substitution of the precursor, ethyl *O*-mesyl-glycolate, with potassium [^{18}F]fluoride/kryptofix 2.2.2, followed by a hydrolysis with aqueous sodium hydroxide solution on Oasis HLB Plus cartridges in the TRACERlab MX_{FDG}.

No-carrier-added aqueous [^{18}F]fluoride solution (1.35 ml, 740 MBq to 14.8 GBq) was added to a reserve vessel in the TRACERlab MX_{FDG}, and then the automated synthesis was started. The [^{18}F]fluoride in enriched ^{18}O water was transferred into a Sep-Pak QMA Light cartridge, which had been converted to the CO_3^{2-} form by treatment with

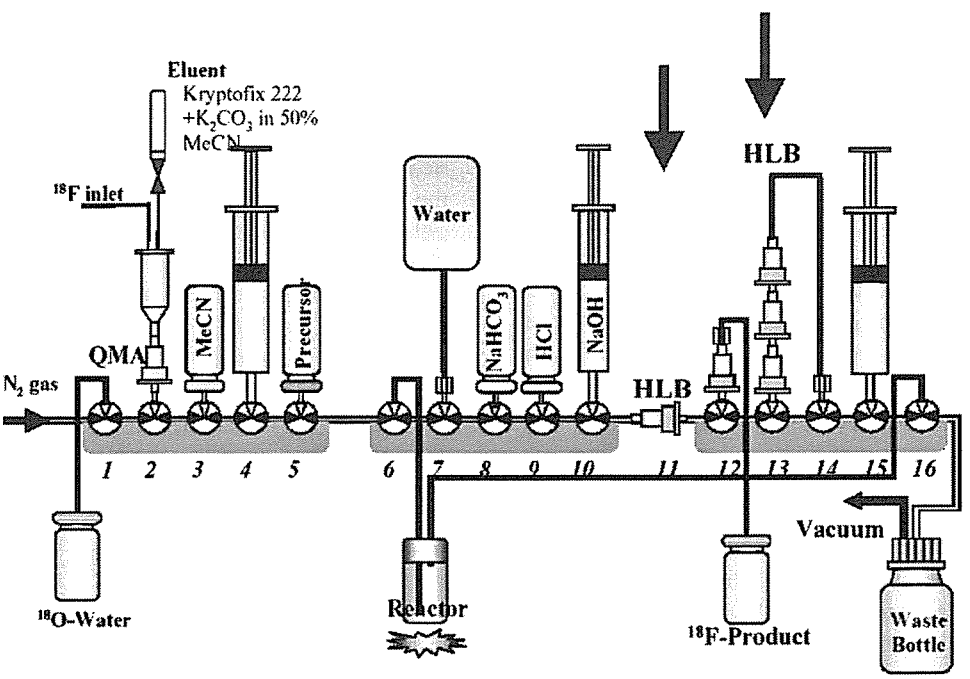

Fig. 2. Schematic diagram of TRACERlab MX_{FDG} for the preparation of sodium [^{18}F]fluoroacetate. Instead of Sep-Pak C-18 cartridges, one Oasis HLB Plus cartridge was placed at position 11 and three at position 13.

an aqueous solution of 0.1 M K_2CO_3. [^{18}F]Fluoride was extracted from the enriched ^{18}O water and trapped on the QMA cartridge, and the enriched ^{18}O water was recovered in the reservoir. A mixed solution of kryptofix 2.2.2 (6.4 mg) in acetonitrile (0.4 ml) and potassium carbonate (0.6 mg) in water (0.3 ml) was employed to elute the trapped [^{18}F]fluoride from the QMA cartridge. The eluate with radioactivity was introduced into the reaction vessel. Water was azeotropically evaporated three times at 95°C under nitrogen gas flow and anhydrous acetonitrile (60 μl×3). After the drying step, 6.2 mg of ethyl *O*-mesyl-glycolate dissolved in 2.2 ml of anhydrous acetonitrile was added to the dried residue in the reaction vessel. The labeling reaction was conducted at 105°C for 5 min in the closed reaction vessel to give rise to ethyl [^{18}F]fluoroacetate. The reaction solution was diluted with 10 ml of distilled water and transferred to Oasis HLB Plus cartridges. The reaction vessel and the cartridges were washed with an additional 30 ml of distilled water to remove the nonreacted [^{18}F]fluoride. The reaction intermediate, ethyl [^{18}F]fluoroacetate, was trapped on the Oasis HLB Plus cartridges. After drying with nitrogen gas flow, 2.7 ml of 1.0 M sodium hydroxide solution was added into the Oasis HLB Plus cartridges, and ethyl [^{18}F]fluoroacetate was base hydrolyzed in the presence of aqueous sodium hydroxide solution. After 5.5 min, the solution in the cartridges was drawn into a 30-ml syringe, and 3 ml of 1.0 M aqueous hydrochloric acid solution was added into the syringe to neutralize the sodium hydroxide. Then, 5 ml of 0.2 M sodium bicarbonate solution was added to adjust the final pH to 5.0–8.0. The solution in the syringe was purified by passage through a Sep-Pak Alumina-N cartridge and filtered through a 0.22-μm sterile filter into a 25-ml sterile vial with 7.4 ml of distilled water. The final solution was analyzed by TLC. The product was also analyzed by HPLC. The total synthesis time was about 32 min.

3. Results and discussion

3.1. Synthesis of ethyl O-mesyl-glycolate

The precursor, ethyl *O*-mesyl-glycolate, was prepared through a nucleophilic substitution reaction. Unlike reported methods [9], instead of using a silica gel column after the reaction, the precursor was directly distilled from the reaction mixture under reduced pressure. This modification simplified the synthesis and avoided introduction of impurities.

3.2. Radiosynthesis of ethyl [^{18}F]fluoroacetate

Ethyl [^{18}F]fluoroacetate is the intermediate produced by the fluorine-18-labeling reaction in the radiosynthesis of sodium [^{18}F]fluoroacetate. During the first attempt to use the complex of K[^{18}F]F and kryptofix 2.2.2 as the nucleophilic agent, we investigated the effects of several reaction conditions, including reaction temperature, reaction time and the amount of the precursor, on the labeling yield.

First, using 60 mg of the precursor dissolved in 2.2 ml of anhydrous acetonitrile, we studied the labeling yield at three temperatures: 75°C, 90°C and 105°C. After the labeling reaction had proceeded for 20 min, the reaction solution was rapidly analyzed by TLC. We conducted three hot runs at each reaction temperature. The labeling efficiencies of ethyl [^{18}F]fluoroacetate were 40.1±8.5%, 57.7±3.6% and 75.4±6.3% at 75°C, 90°C and 105°C, respectively. As a result, a reaction temperature of 105°C was chosen for the radiosynthesis.

Next, we investigated the labeling reaction at four different reaction times (5, 10, 15 and 20 min) in the presence of 60 mg precursor at 105°C. Thin-layer chromatography analyses revealed that the labeling efficiency of the substitution reaction was more than 70% for all four reaction times (Table 2). So a reaction time of 5 min was chosen for the labeling reaction.

Finally, the amount of the precursor needed was evaluated. Using 6.2, 30 and 60 mg of the precursor at 105°C and a reaction time of 5 min, the labeling efficiencies by fluorine-18 were 71.8±8.7% (n=3), 70.5±3.6% (n=3) and 73.4±2.7% (n=3), respectively. As a result, the smallest amount, 6.2 mg, was chosen.

Based on our past experience, the amounts of kryptofix 2.2.2 and potassium carbonate used were 6.4 and 0.6 mg, respectively, in each run in the synthesis. Reduction in the amount of potassium carbonate and kryptofix 2.2.2 did not affect the labeling efficiency.

3.3. Purification and hydrolysis of ethyl [^{18}F]fluoroacetate

As done during the synthesis of [^{18}F]FDG in the TRACERlab MX_{FDG}, we purified the intermediate before its hydrolysis. First, the ethyl [^{18}F]fluoroacetate intermediate was trapped on the reversed phase cartridges. Cartridges containing radioactivity were washed with 30 ml of distilled water to remove nonreacted [^{18}F]fluoride anion, acetonitrile and kryptofix 2.2.2. In the case of [^{18}F]FDG synthesis, two Sep-Pak C18 cartridges were used in this step, and most of the radioactivity was extracted by the cartridges. However, only 3–5% of the radioactivity was trapped when Sep-Pak C18 cartridges were used in the preparation of sodium [^{18}F]fluoroacetate. In previous reports [17,18], Oasis HLB Plus cartridges had higher capacity and selectivity than Sep-Pak C18 cartridges. By using two Oasis HLB Plus

Table 2
The effect of reaction time on the labeling efficiency of ethyl [^{18}F]fluoroacetate

Time (min)	Labeling Efficiency (%)
5	73.4±2.7
10	72.7±6.0
15	70.1±4.8
20	75.4±6.3

The precursor (60 mg) was dissolved in anhydrous CH_3CN (2.2 ml) and heated at 105°C. The labeling reaction was performed three times in each reaction time.

cartridges instead of two Sep-Pak C18 cartridges, the extraction efficiencies improved to 27.2±2.8%. To avoid the dead volume of a larger cartridge (500 mg or larger), we employed multiple Oasis HLB Plus cartridges of the smaller size (225 mg) to increase recovery of the intermediate. When three Oasis HLB Plus cartridges were used, one at position 11 and two at position 13, the extraction efficiencies improved to 43.1±2.2%. Using four, five or six Oasis HLB Plus cartridges all improved the efficiency to greater than 50%. As a consequence, we decided to use four Oasis HLB Plus cartridges, one at position 11 and three at position 13, as shown in Fig. 2.

Following the purification, the hydrolysis of ethyl [^{18}F]fluoroacetate was carried out on the cartridges. For [^{18}F]FDG synthesis, this hydrolysis is accomplished at room temperature. Although the hydrolysis of ethyl [^{18}F]fluoroacetate was reported to be performed at 60°C in 3 ml of 1 M aqueous potassium hydroxide solution in a previous paper [9], we anticipated that the hydrolysis of ethyl [^{18}F]fluoroacetate on the cartridges also might proceed at room temperature. Therefore, we examined the hydrolysis of ethyl [^{18}F]fluoroacetate on the cartridges at two temperatures, 60°C and room temperature, and obtained the kinetic curves of hydrolysis (data not shown). In the presence of 1.0 M sodium hydroxide, ethyl [^{18}F]fluoroacetate was completely hydrolyzed in 3.5 min at 60°C and 5.5 min at room temperature. Because longer than 5.5 min was never required, the hydrolysis of ethyl [^{18}F]fluoroacetate was performed at room temperature for 5.5 min.

Because more HLB Plus cartridges were being used, the amount of aqueous sodium hydroxide was increased to 2.7 ml based on experimental results. The concentration of aqueous sodium hydroxide solution, 1.0 M [19], was used without further investigation. About 3.0 ml of 1.0 M aqueous hydrochloric acid solution was required to neutralize the base. The pH of the final solution was adjusted to 5.0–8.0 with 5 ml of 0.2 M aqueous sodium bicarbonate solution, instead of the citrate buffer solution used in the [^{18}F]FDG synthesis.

3.4. Influence of initially added radioactivity

In the present work, different amounts of fluorine-18 radioactivity, from 740 MBq to 14.8 GBq, were used in the radiosynthesis. Radiochemical yields (decay corrected) were calculated to be 49.7±6.0%, 50.9±6.1%, 49.5±5.6% and 50.3±3.7%, in the cases of 740 MBq, 33.7 GBq, 7.4 GBq and 14.8 GBq, respectively (n=3). The data indicate that the radiochemical yield of the final product, sodium [^{18}F]fluoroacetate, did not depend on the initial amount of fluorine-18 radioactivity.

3.5. Analyses of sodium [^{18}F]fluoroacetate

The final solution was analyzed by TLC and HPLC. No fluorine-18 anion was detected in the final solution, and the radiochemical purity of sodium [^{18}F]fluoroacetate was confirmed to be more than 99%. The total radiochemical yield was 50.2±4.8% (n=10, decay corrected). The chemical purity was also assessed by HPLC, and no specific peaks were found except for that of sodium bicarbonate. The pH of the final solution was 7.5±0.2. The total synthesis time was about 32 min. The final solution was also analyzed with GC to show that it contained less than 10 ppm acetonitrile. The pyrogenicity check was carried out using an LAL kit and showed satisfactory results. The absence of Kryptofix 2.2.2 was confirmed with a previously reported method [20]. All the results from the preparation of sodium [^{18}F]fluoroacetate using the TRACERlab MX_{FDG} presented here showed dramatic improvement compared to previous works [9–12].

4. Conclusion

The automated synthesis of sodium [^{18}F]fluoroacetate has been successfully accomplished. Using the commercial [^{18}F]FDG synthesizer TRACERlab MX_{FDG}, the final solution can be obtained in 32 min after EOB with a radiochemical yield of 50.2±4.8% (decay corrected). This work widens the application of the TRACERlab MX_{FDG} and should provide users of the TRACERlab MX_{FDG} with easy access to sodium [^{18}F]fluoroacetate for PET imaging.

Acknowledgments

We are grateful to Mr. S. Nakakoji and Mr. K. Hanawa who produced [^{18}F]fluoride for this work, and Mr. S. Kasamatsu for the expert technical assistance. This work was supported by The 21st Century Centers of Excellence Program by Japan Society for the Promotion Science (JSPS), "Biomedical Imaging Technology Integration Program (BITIP)," and by the Research and Development Project Aimed at Economic Revitalization (Leading Project) by the Ministry of Education, Culture, Sports, Technology and Science (MEXT), Japan.

References

[1] Eason CT, Wickstrom M, Turck P, Wright GRG. A review of recent regulatory and environmental toxicology studies on 1080. NZ J Ecol 1999;23(2):129–37.
[2] Guidelines for the safe use of sodium fluoroacetate (1080). New Zealand: Department of Labor; 2002.
[3] Liebecq C, Peters RA. The toxicity of fluoroacetate and the tricarboxylic acid cycle. Biochem Biophys Acta 1949;3:215–30.
[4] Clarke DD. Fluoroacetate and fluorocitrate: mechanism of action. Neurochem Res 1991;16(9):1055–8.
[5] Lear JL, Ackermann RF. Evaluation of radiolabeled acetate and fluoroacetate as potential tracers of cerebral oxidative metabolism. Metab Brain Dis 1990;5(1):45–56.
[6] Ponde DE, Oyama N, Dence CS, Welch MJ. [^{18}F]fluoroacetate, an analog of C-11 acetate for tumor imaging. J Nucl Med 2003; 44:1062P.
[7] Oyama N, Ponde DE, Dence CS, Yokoyama O, Siegel BA, Welch MJ. In vitro and in vivo assessment of F-18 fluoroacetate; a potential analog for tumor imaging. J Nucl Med 2004;45:331P.

[8] Matthies A, Ezziddin S, Ulrich EM, Palmedo H, Biersack HJ, Bender H, et al. Imaging of prostate cancer metastases with ^{18}F-fluoroacetate using PET/CT. Eur J Nucl Med Mol Imaging 2004;31(5):797.

[9] Jeong JM, Lee DS, Chung JK, Lee MC, Koh CS, Kang SS. Synthesis of no-carrier-added [^{18}F]fluoroacetate. J Label Compd Radiopharm 1997;39:395–9.

[10] Sykes TR, Ruth TJ, Adam MJ. Synthesis and murine tissue uptake of sodium [^{18}F]fluoroacetate. Int J Radiat Appl Instrum B 1986;13(5): 497–500.

[11] Tewson TJ, Welch MJ. Preparation and preliminary biodistribution of NCA fluorine-18 fluoroethanol. J Nucl Med 1980;20:559–64.

[12] Bosch AL, Degrado TR, Gatley SJ. Preparation of no carrier added fluorine-18 labeled 16-fluorohexadecanoic and fluoroacetic acids from highly reactive tetraethylammonium [^{18}F]fluoride. Int J Radiat Appl Instrum A 1986;37(4):305–8.

[13] Fuchtner F, Steinbach J, Mading P, Johannsen B. Basic hydrolysis of 2-[^{18}F]Fluoro-1,3,4,6- tetra-*O*-acetyl-D-glucose in the preparation of 2-[^{18}F]Fluoro-2-deoxy-D-glucose. Appl Radiat Isot 1996;47:61–6.

[14] From the website of GE Healthcare. http://www.gehealthcare.com/usen/fun_img/radiopharmacy/products/tracerlabmx.html.

[15] Havbrandt O, Wachtmeister CA. Synthesis of mesyloxyacetic acid and some derivatives. Acta Chem Scand 1968;22:2043–4.

[16] Tasic L, Abraham RJ, Rittner R. Substituent effects on ^{1}H and ^{13}C NMR chemical shifts in α-monosubstituted ethyl acetates: principal component analysis and ^{1}H chemical shift calculations. Magn Reson Chem 2002;40:449–54.

[17] Ponde DE, Dence CS, Schuster DP, Welch MJ. Rapid and reproducible radiosynthesis of [^{18}F]FHBG. Nucl Med Biol 2004;31: 133–8.

[18] Lemaire C, Damhaut P, Lauricella B, Mosdzianowski C, Morelle J-L, Monclus M, et al. Fast [^{18}F]FDG synthesis by alkaline hydrolysis on a low polarity solid phase support. J Label Compd Radiopharm 2002; 45:435–47.

[19] Mosdzianowski C, Lemaire C, Simoens F, Aerts J, Morelle J-L, Luxen A. Epimerization study on [^{18}F]FDG produced by an alkaline hydrolysis on solid support under stringent conditions. Appl Radiat Isot 2002;56:871–5.

[20] Mock BH, Winkle W, Vavrek MT. A color spot test for the detection of Kryptofix 2.2.2 in [^{18}F]FDG preparations. Nucl Med Biol 1997;24: 193–5.

資料(6)

Available online at www.sciencedirect.com

SCIENCE DIRECT®

Nuclear Medicine and Biology 33 (2006) 281–286

NUCLEAR MEDICINE — AND — BIOLOGY

www.elsevier.com/locate/nucmedbio

Automatic synthesis of 16α-[^{18}F]fluoro-17β-estradiol using a cassette-type [^{18}F]fluorodeoxyglucose synthesizer

Tetsuya Mori[a,*], Shingo Kasamatsu[b], Christoph Mosdzianowski[c], Michael J. Welch[d], Yoshiharu Yonekura[a], Yasuhisa Fujibayashi[a]

[a]*Biomedical Imaging Research Center, University of Fukui, Matsuoka, Fukui 910-1193, Japan*
[b]*JFE P&S Fukui Branch, University of Fukui, Matsuoka, Fukui 910-1193, Japan*
[c]*GE Healthcare Technologies, Parc Scientifique du Sart Tilman Av. Pre-Aliy (c/o Socran) B-4031 Lieage, Belgium*
[d]*Mallinckrodt Institute of Radiology, Washington University Medical Center, St. Louis, MO 63110, USA*

Received 22 March 2005; received in revised form 2 November 2005; accepted 6 November 2005

Abstract

16α-[^{18}F]fluoro-17β-estradiol ([^{18}F]FES) is a radiotracer for imaging estrogen receptors by positron emission tomography. We developed a clinically applicable automatic preparation system for [^{18}F]FES by modifying a cassette-type [^{18}F]fluorodeoxyglucose synthesizer. Two milligrams of 3-*O*-methoxymethyl-16,17-*O*-sulfuryl-16-epiestriol in acetonitrile was heated at 105°C for 10 min with dried [^{18}F]fluoride. The resultant solution was evaporated and hydrolyzed with 0.2 N HCl in 90% acetonitrile/water at 95°C for 10 min under pressurized condition. The neutralization was carried out with 2.8% $NaHCO_3$, and then the high-performance liquid chromatography (HPLC) purification was performed. The desired radioactive fraction was collected and the solvent was replaced by 10 ml of saline, and then passed through a 0.22-μm filter into a pyrogen-free vial as the final product. The HPLC purification data demonstrated that [^{18}F]FES was synthesized with a yield of 76.4±1.9% (n=5). The yield as the final product for clinical use was 42.4±3.2% (n=5, decay corrected). The total preparation time was 88.2±6.4 min, including the HPLC purification and the solvent replacement process. The radiochemical purity of the final product was >99%, and the specific activity was more than 111 GBq/μmol. The final product was stable for more than 6 h in saline containing sodium ascorbate. This new preparation system enables us to produce [^{18}F]FES safe for clinical use with high and reproducible yield.

Keywords: [^{18}F]FES; Estrogen receptors; Automatic synthesis; Radiopharmaceutical; PET; Cassette-type FDG synthesizer

1. Introduction

The estrogen receptor (ER) status is an important prognostic factor in breast cancer because the ER positive cancers are less aggressive in clinical course and likely to respond to hormonal therapy [1]. The ER expression can be estimated with biopsied material; however, sampling errors may occur when patients have large or multisite tumors. 16α-[^{18}F]fluoro-17β-estradiol ([^{18}F]FES) has been developed as a tracer for imaging ER by positron emission tomography (PET) [2,3]. In clinical studies, the uptakes of [^{18}F]FES were proportional to the ER concentration in both primary and metastatic breast cancers [4–7]. FES-PET information may predict the response of the advanced breast cancer to hormonal therapy and may be useful for guiding better treatment. Therefore, [^{18}F]FES is one of the most promising radiopharmaceutical for monitoring of ER status in breast cancer; however, it is not widely used because of the difficulty of the synthesis. The first synthesis of [^{18}F]FES was reported by Kiesewetter et al. [8], and the application of robotic synthesis was evolved [9]. Their procedure involved reduction by $LiAlH_4$ and liquid N_2. Another procedure was reported, which uses 3-*O*-methoxymethyl-16,17-*O*-sulfuryl-16-epiestriol (**1**) as a precursor [10,11]. The advantages of the latter procedure are that the nucleophilic substitution by [^{18}F]fluoride proceeded rapidly with good yield, and this precursor is commercially available. It is also advantageous that the hydrolysis reactions were performed under mild condition [12]. Although the automatic synthesis of [^{18}F]FES using

* Corresponding author. Tel.: +81 776 61 8491; fax: +81 776 61 8170.
E-mail address: morit@fmsrsa.fukui-med.ac.jp (T. Mori).

0969-8051/$ – see front matter © 2006 Published by Elsevier Inc.
doi:10.1016/j.nucmedbio.2005.11.002

[^{18}F]fluorodeoxyglucose (FDG) synthesis module was reported [13], reproducible yield of [^{18}F]FES could not be realized because of the complex reaction conditions and purification processes.

[^{18}F]fluorodeoxyglucose synthesis has become a standard practice in clinical PET centers for diagnosis of cancer. To make a radiotracer to be widely used, it is necessary to establish a system that can produce high-quality product with the operation easy enough for routine work. We chose TRACERlab MX_{FDG} as the module for [^{18}F]FES synthesis because it is widely used as a simple automatic FDG synthesizer and it has the flexibility in programming and accepts modification to the cassette. However, this module does not have a cooling function, and the cassette has low chemical resistance. In this study, we studied the hydrolysis condition on this module and performed the synthesis without changing the hardware, and also established a formula of high-quality product for clinical use.

2. Materials and methods

2.1. Reagents and equipment

All chemicals were obtained from commercial sources and used without further purification. The precursor (**1**) and the authentic 16α-fluoro-17β-estradiol were purchased from ABX (Radeberg, Germany). The sodium bicarbonate solution and the sodium ascorbate solution used were of pharmaceutical grade. The other reagents and solvents were obtained from Sigma-Aldrich (St. Louis, MO). The synthesis was performed using TRACERlab MX_{FDG} (GE Medical Systems, Milwaukee, WI), which is one of the automatic FDG synthesizers. The high-performance liquid chromatography (HPLC) system was consisted of a pump (LC-10AD, Shimadzu, Kyoto, Japan), a UV detector (SPD-10AVP, Shimadzu) and a NaI(Tl) radioactive detector (RLC-700, Aloka, Tokyo, Japan).

2.2. Process of [^{18}F]FES preparation

The total procedure of [^{18}F]FES preparation consisted of four steps as follows: (a) fluorination, (b) hydrolysis, (c) HPLC purification and (d) formulation (Fig. 1). The automatic synthesis of [^{18}F]FES including Steps a and b were performed on TRACERlab MX_{FDG}. The diagram of the [^{18}F]FES preparation system is shown in Fig. 2.

2.2.1. Synthesis module

TRACERlab MX_{FDG} is a disposable cassette-type module realizing easy modification of chemical process as well as easy operation as routine work without requiring expert knowledge in chemistry. The synthesis program consists of a Microsoft Excel file defining synthesis parameters such as temperature, time, vacuum pressure, three-way cocks and syringe positions.

2.2.2. Preparation of reagents and cassette

The reagents for [^{18}F]FES synthesis were contained in a set of six vials. The content of each vial was as follows: A, 22 mg of Kryptofix 2.2.2 and 7 mg of potassium carbonate mixture in 50% acetonitrile/water (0.6 ml); B, anhydrous acetonitrile (2 ml); C, 2 mg of the precursor in anhydrous acetonitrile (2 ml); D, 0.2 N hydrochloric acid in 90% acetonitrile/water (2 ml); E, 2.8% sodium bicarbonate in water (2 ml); and F, 70% ethanol/water (2 ml). The reagents, except for A, were sealed in standard 10-ml glass vials. The reagent A in 1.2-ml vial was the same to the one used in FDG synthesis.

The cassette was prepared from the FDG synthesis cassette with a little modification keeping aseptic condition (Fig. 2). The alumina N and two C18 Sep-Pak cartridges,

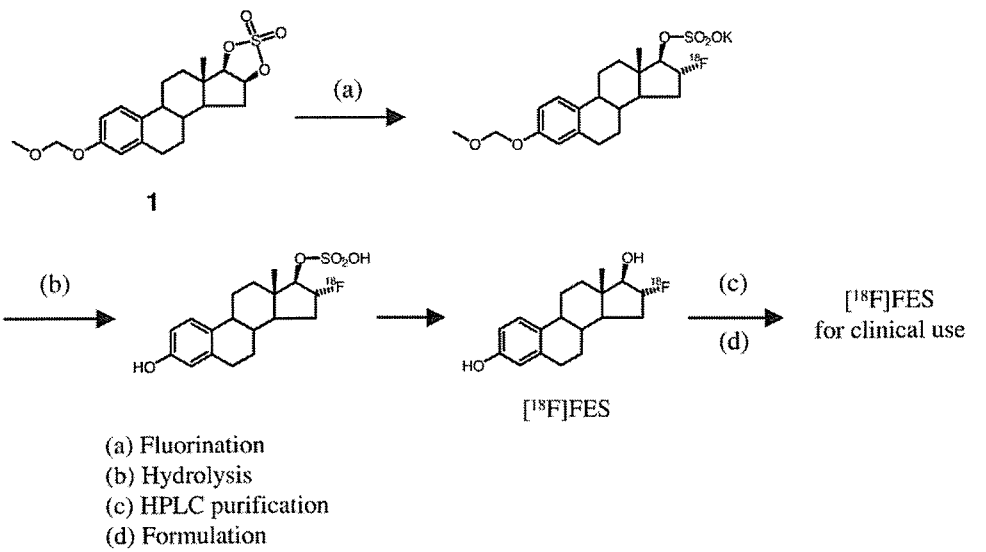

Fig. 1. Scheme of [^{18}F]FES synthesis for clinical use starting from **1**.

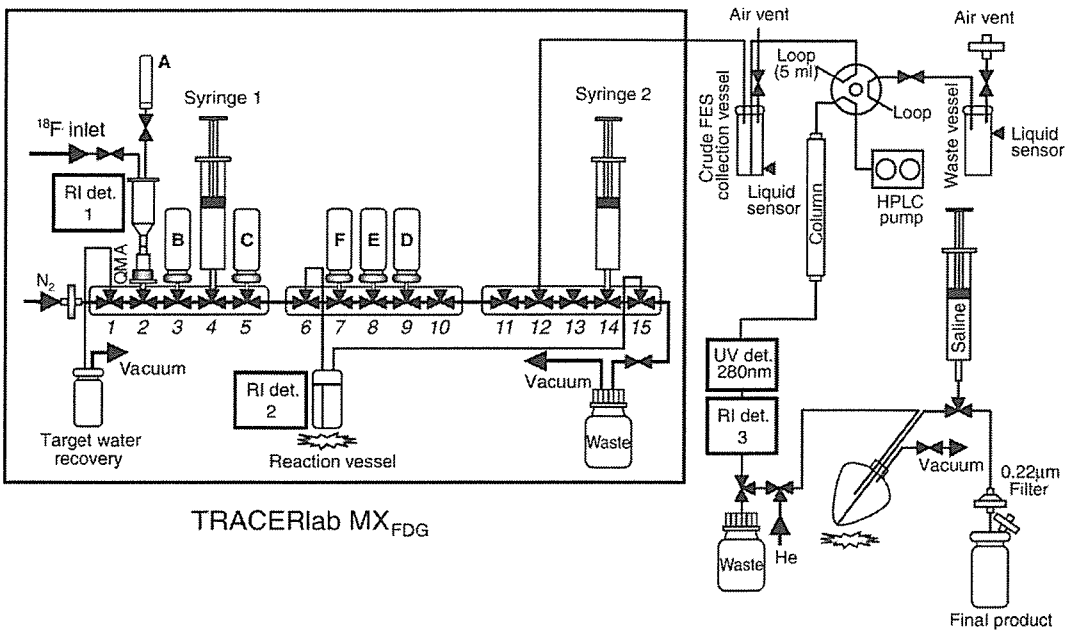

Fig. 2. Schematic diagram of the [^{18}F]FES preparation system for clinical use.

unnecessary for [^{18}F]FES synthesis, were removed from the cassette. The water bag connection tube, attached at position 7, was utilized for the central and right manifold connection (positions 10 and 11) after adjustment of the tube length. To add another vial, we moved the male-to-male connector, which had been attached to the C18 Sep-Pak, to position 7 and connected it to an 18G needle. Prior to the synthesis, an activated QMA Sep-Pak light cartridge and two 30-ml polyethylene syringes were jointed to the cassette.

2.2.3. Synthesis of [^{18}F]FES

The synthesis of [^{18}F]FES was modified from the method of Römer et al. [12]. Fluorine-18 was produced by the ^{18}O(p,n)^{18}F reaction using an ultrasmall cyclotron OSCAR (JFE P&S/Oxford, Yokohama, Japan) or RDS eclipse RD/HP (Siemens/CTI, Knoxville, TN) in the PET center of the University of Fukui. The irradiated ^{18}O water, which contained a carrier-free [^{18}F]fluoride, was transferred to the module automatically and passed through the QMA cartridge. The trapped [^{18}F]fluoride on the cartridge was eluted by A into the reaction vessel and dried three times adding small amount of B. The precursor in acetonitrile, C, was added to the reaction vessel for fluorination and heated at 105°C for 10 min. After the fluorination, the solution was transferred to the syringe 1 to release the increased pressure and then returned back to the reaction vessel. The solvent was evaporated to decrease the total volume. To start the hydrolysis, we added D to the reaction vessel and heated it at 95°C for 10 min with the valves closed, which brought a pressurized condition. To stop the hydrolysis, we performed neutralization in syringe 1. The base reagent, E, was transferred to syringe 1 during the hydrolysis, and then the reaction solution was drawn in the same syringe. The mixture was pushed out to the reaction vessel to recover the remaining radioactivity and was drawn again. The radioactive solution was pushed out into the crude FES collection vessel for HPLC purification. The acetonitrile in B (about 1 ml) was used to flush the reaction vessel and the cassette, and added to the crude FES vessel. The reagent F was used for flushing the cassette.

2.2.4. The HPLC purification and the formulation steps

The HPLC purification was performed using a Cosmosil 5C_{18}-AR-2 column (20-mm ID×250-mm, Nacalai Tesque, Kyoto, Japan) with acetonitrile/water/ethanol (30:40:30) at a flow rate of 6.0 ml/min. For the HPLC injection, we used a 5-ml sample loop and automatic injector (Rheodyne, Rohnert Park, CA). The desired radioactive fraction was collected in a round-bottom flask containing 0.1 ml of sodium ascorbate (250 mg/ml) in the solvent replacement unit (JFE P&S). The solvent was removed in vacuo and the residue was dissolved in 10 ml of saline, and then passed through a sterile 0.22-μm filter (Millex-GS, Millipore, MA) to a pyrogen-free vial as the final product.

2.3. Evaluation of the products

The radiochemical purity of the product right after the synthesis and in the final product for clinical use was determined by HPLC analysis using a Cosmosil 5C_{18}-MS-2 column (4.6-mm ID×150 mm, Nacalai Tesque) with 40% acetonitrile/water at a flow rate of 1.0 ml/min. In this system, [^{18}F]FES was eluted for 8.1 min. To determine the yield of fluorination, we measured the free [^{18}F]fluoride in the crude [^{18}F]FES solution by radio thin-layer chromatography (radio TLC) method. The radio TLC was performed on Merck aluminum backed silica gel 60 plates with chloroform/methanol (4:1). The Rf values of [^{18}F]fluoride

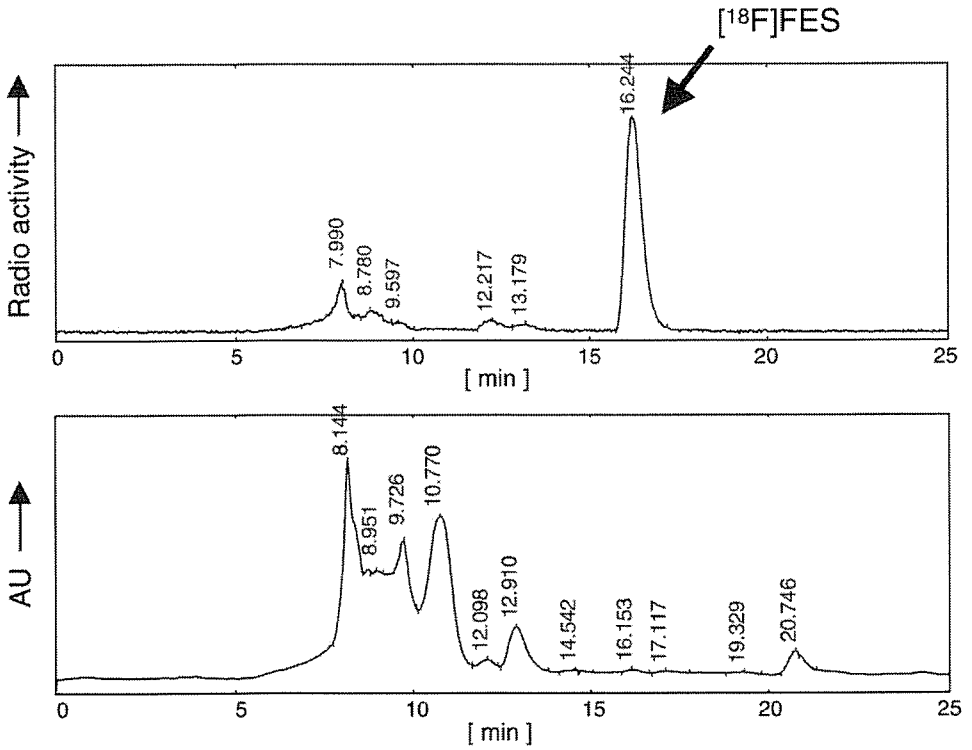

Fig. 3. The chromatograms of the crude [^{18}F]FES at the HPLC purification. Top, radioactivity; bottom, UV absorbance at 280 nm. The retention time of [^{18}F]FES was 16.2 min, which corresponded to the authentic unlabeled 16α-fluoro-17β-estradiol.

and [^{18}F]FES were 0.00 and 0.75, respectively. The other two unknown labeled compounds had Rf values of 0.30 and 0.40.

3. Results and discussion

In this study, we established the optimal procedure for [^{18}F]FES preparation for clinical use through investigating the condition for the synthesis, the purification and the formulation steps. We chose the synthesis method using **1** as the precursor because the reaction can be carried out under mild condition, which is suitable for our module. In addition, **1** is commercially available. The process of [^{18}F]FES synthesis is outlined in Fig. 1. Steps a and b were performed in TRACERlab MX_{FDG}. There were only three points different between the [^{18}F]FES synthesis and the FDG synthesis as follows: the synthesis program, the regents and the cassette layout. The advantage of this method was that the synthesis of [^{18}F]FES and FDG can be performed using the same machine without a change to the hardware.

The fluorination of **1** was performed by the nucleophilic substitution reaction by $K^{18}F$ and accomplished with high yield (89.5±0.8%, n=5). The next hydrolysis step consists of two consecutive reactions. Römer et al. [12] reported two methods of the hydrolysis for their automated module: the pressure hydrolysis method using HCl and the multiple azeotropic evaporation method using hydrochloric acetonitrile. They recommended the latter because it had an advantage of removing the acid and the unreacted [^{18}F]fluoride at the same time. We tried this method, but the radioactivity in the reaction vessel varied between the different runs (40.0±27.3%, n=5). We suspected that the main reason for the inconsistency was decomposition of [^{18}F]FES during the azeotropic evaporation, though it might have depended on the module we used. As it seemed that the decomposition occurred under water-rich condition, we

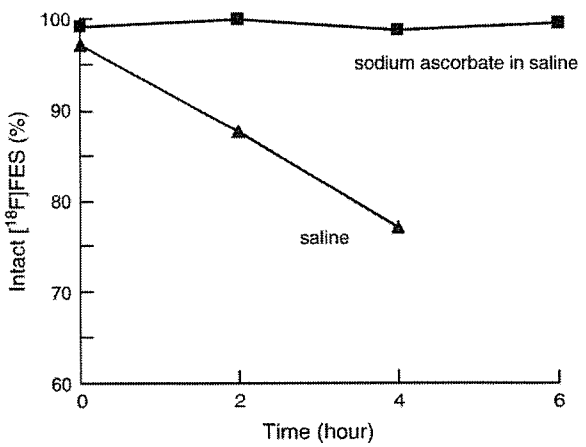

Fig. 4. The stability of [^{18}F]FES in the final product for clinical use. 16α-[^{18}F]fluoro-17β-estradiol was rapidly degraded in saline without sodium ascorbate.

speculated that maintaining acetonitrile/water ratio during the reaction would lead to high and reproducible yield of [^{18}F]FES. In order to keep the acetonitrile component, we carried out the reaction using 90% hydrochloric acetonitrile in closed valve condition. In this condition, [^{18}F]FES was formed within 6 min after the start of hydrolysis at 95°C, and the yield reached the plateau level within another 4 min. Therefore, we decided the reaction time to be 10 min. In this way, most of the radioactivity in the reaction vessel was maintained during the hydrolysis. Fig. 3 shows the chromatogram of the HPLC purification. The retention time of [^{18}F]FES was 16.2 min, which corresponded to that of unlabeled authentic FES. The chromatogram demonstrated that the [^{18}F]FES synthesis was accomplished with a yield of 76.4±1.9% based on the crude [^{18}F]FES solution (n=5). It indicated that the fluorination and the hydrolysis were achieved properly. This method realized sufficiently high and reproducible yields for clinical use as we had intended. The volume of the crude [^{18}F]FES solution was about 3 ml without the reagent F, and the pH of this solution was 8. The purified [^{18}F]FES was stable when the mobile phase of HPLC contained 30% ethanol.

The formula of the final product was also examined. Several researchers provided the final product of [^{18}F]FES as an ethanol/saline solution, probably because of easy preparation from HPLC eluate and high lipophilicity of [^{18}F]FES. However, ethanol causes unacceptable side effects in some patients. Thus, we attempted to prepare the final product as saline solution. However, the radiochemical purity of the product declined rapidly. The percentage of intact [^{18}F]FES was 87% at 2 h (Fig. 4). It indicated that ethanol might be working not only as a solvent but also as a radical scavenger. When sodium ascorbate was added as a radical scavenger instead of ethanol to prevent the decomposition, the radiochemical purity of [^{18}F]FES in saline was over 98% after 6 h. In the filtering process, about 10% of the radioactivity based on input [^{18}F]fluoride was trapped on the membrane filter. Fortunately, the final product through the filter was not trapped much in the final glass vial and the polyethylene syringe used for injection. The radioactivity trapped on the filter could be eluted by 70% ethanol and was confirmed as an intact [^{18}F]FES. Even though our formula causes the decrease of the final product in the filtering process, however, it has the advantage of avoiding the side effects in clinical use. The final product was obtained with a yield of 42.4±3.2% based on input [^{18}F]fluoride (decay corrected, n=5). The specific activity was calculated by the analytical HPLC system (the detection limit was 0.1 μg/ml), and the value was more than 111 GBq/μmol.

The total preparation time was 88.2±6.4 min. The automated synthesis on TRACERlab MX_{FDG} was completed in 50 min. The HPLC purification took 20 min, and another 20 min was required for the formulation process. If the final product was prepared in ethanol/saline solution like in other reports, the ethanol/water solution can be used as the mobile phase in purification, and the following formulation process can be omitted.

4. Conclusion

In this study, we demonstrated that the [^{18}F]FES for clinical use can be prepared with high and reproducible yield using a commercial FDG synthesizer. The merit of our method is that [^{18}F]FES can be easily prepared in a PET institution without a chemist because it does not require expertise in chemistry. Our preparation system enables routine use of [^{18}F]FES in clinical PET centers.

Acknowledgments

We thank Hirokazu Hanawa and Toshinao Nakakoji for operating the CTI cyclotron. Part of this study was supported by the Research and Development Project Aimed at Economic Revitalization from the Ministry of Education, Culture, Sports, Science and Technology (MEXT), Japan; the 21st Centry COE program "Biomedical Imaging Technology Integration Program" from the Japan Society of the Promotion of Science (JSPS); and a grant for the Collaboration of Regional Entities for the Advancement of Technological Excellence (CREATE) from the Japan Science and Technology Agency (JST).

References

[1] Vollenweider-Zerargui L, Barrelet L, Wong Y, Lemarchand-Beraud T, Gomez F. The predictive value of estrogen and progesterone receptors' concentrations on the clinical behavior of breast cancer in women: clinical correlation on 547 patients. Cancer 1986;57:1171–80.

[2] Kiesewetter DO, Kilbourn MR, Landvatter SW, Heiman DF, Katzenellenbogen JA, Welch MJ. Preparation of four fluorine-18 labeled estrogens and their selective uptakes in target tissue of immature rats. J Nucl Med 1984;25:1212–21.

[3] Katzenellenbogen JA, Welch MJ, Dehdashti F. The development of estrogen and progestin radiopharmaceuticals for imaging breast cancer. Anticancer Res 1997;17:1573–6.

[4] Dehdashti F, Flanagan FL, Mortimer JE, Katzenellenbogen JA, Welch MJ, Siegel BA. Positron emission tomographic assessment of "metabolic flare" to predict response of metastatic breast cancer to antiestrogen therapy. Eur J Nucl Med 1999;26:51–6.

[5] Mintun MA, Welch MJ, Siegel BA, Mathias CJ, Brodack JW, McGuire AH, et al. Breast cancer: PET imaging of estrogen receptors. Radiology 1988;169:45–8.

[6] McGuire AH, Dehdashti F, Siegel BA, Lyss AP, Brodack JW, Mathias CJ, et al. Positron tomographic assessment of 16α-[^{18}F]fluoro-17β-estradiol uptake in metastatic breast carcinoma. J Nucl Med 1991;32:1526–31.

[7] Dehdashti F, Mortimer JE, Siegel BA, Griffeth LK, Bonasera TJ, Fusselman MJ, et al. Positron tomographic assessment of estrogen receptors in breast cancer: comparison with FDG-PET and in vitro receptor assays. J Nucl Med 1995;36:1766–74.

[8] Kiesewetter DO, Katzenellenbogen JA, Kilbourn MR, Welch MJ. Synthesis of 16-fluoroestrogens by unusually facile fluoride ion displacement reactions: prospects for the preparation of fluorine-18 labeled estrogens. J Org Chem 1984;49:4900–5.